Hydrological drought prediction and its influencing

2 factors features analysis based on a machine learning

3 model

- 4 Min Li^{1,2}, Yuhang Yao¹, Zilong Feng³, Ming Ou¹
- ¹College of Hydraulic Science and Engineering, Yangzhou University, Yangzhou, China, 225000
- 6 ²State Key Laboratory of Water Disaster Prevention, China, 210000
- JiLin Province Water Resource and Hydropower Consultative Company of P.R CHINA, Changchun,
- 8 China, 130012
- 9 Correspondence to: Min Li (limintju@126.com)
- 10 Abstract: Predicting future drought conditions isare crucial for effective disaster management.
- 11 In this study, a machine learning framework is proposed to predict hydrological drought in the Huaihe
- 12 River Basin, China. The interpretable Extreme Gradient Boosting (XGBoost) model is applied to
- 13 <u>forecastpredict</u> four drought categories in 28 grid regions for one-month <u>forecastingprediction(forecast</u>
- 14 <u>horizon T=1)</u>, using 26 factors features for monthly and 18 for seasonal predictions. The framework also
- 15 integrates the Shapley Additive Explanation (SHAP) variable importance index to infer drought
- prediction <u>featuresfactors</u>. The model achieves 79.9% accuracy in classifying droughts, with the Standard
- Precipitation Index (SPI) being the most influential factor feature. The SHAP values of SPI are 0.360,
- 18 0.261, 0.169, and 0.247 for spring, summer, autumn, and winter, respectively. Soil moisture content and
- 19 evapotranspiration are particularly affected in spring and autumn, while large-scale climatic
- 20 <u>featuresfactors</u> are more significant in summer and winter. Overall, this study offers valuable decision
- ${\bf 21} \qquad {\bf support} \ {\bf for} \ {\bf regional} \ {\bf drought} \ {\bf management} \ {\bf and} \ {\bf water} \ {\bf resource} \ {\bf allocation}.$
- 22 Keywords: XGBoost; SHAP; Drought prediction; SRI; Huaihe River Basin

23 1 Introduction

- 24 Drought is a global disaster characterized by its long duration and extensive impacts, resulting in
- 25 severe implications for the economy, agriculture, and environment (Fu et al., 2018; Shi et al., 2018; Zhou
- et al., 2020; 2021). Over the past 20 years, the frequency and severity of global drought events have
- 27 increased (Dai 2011; 2012; 2013; Zhang et al., 2019), affecting water security, economic growth, and
- 28 food supply in some areas. Therefore, drought prediction is of great significance for managing water

设置了格式: 字体: (默认) Times New Roman, (中文) 宋体, 10 磅 resources and reducing losses caused by drought.

Consequently, according to the different effects of drought, previous studies have divided it into several different types. Among them, four types of droughts are widely used: meteorology, hydrology, agriculture, and social economy (Wilhite and Glantz, 1985; American Meteorological Society, 2013). In the past few decades, more than one hundred drought indices based on single or multiple hydroclimatic variables have been proposed to represent different drought characteristics. For example, the Palmer Drought Severity Index (PDSI) (Palmer 1965), the Standardized Precipitation Index (SPI) (McKee et al., 1993), and the Standardized Runoff Index (SRI) (Shukla and Wood, 2008). SPI index and SRI index are robust, statistically straightforward to compute, and well-suited to long-term time series data. Therefore, this study chooses the SPI index and SRI index to characterize meteorological drought and hydrological drought.

In recent years, there has been an increasing trend toward utilizing machine learning to predict droughts (Ardabili et al., 2020; Sun and Scanlon, 2019). Compared to conventional regression models, machine learning-based models better capture the non-linear characteristics inherent in drought problems and exhibit more robustness, especially when dealing with high-dimensional datasets (Mishra and Singh, 2010; Kikon and Deka, 2022; Prodhan et al., 2022; Wu et al., 2022). Multiple machine learning models such as artificial neural networks (Orimoloye et al., 2021; Orimoloye et al., 2022), support vector machines (Li et al., 2021), random forests(Park et al., 2019), and extreme gradient boosting (XGBoost) (Choi et al. 2018; Han et al. 2019; Zhang et al., 2023) have been extensively employed in the research field of drought. Machine Learning models can learn the input-output relationships in training data and can effectively leverage big data to improve prediction accuracy (Mardian et al., 2023). By training treebased machine learning models, Bachmair et al. (2016) discovered that tree-based machine learning models outperform baseline models. Jungho and Kim (2023) employed a tree-structured XGBoost model to predict the likelihood of impact occurrence (LIO) of drought on public water supply. Their findings demonstrated that the XGBoost model exhibited high accuracy and low uncertainty. Furthermore, the XGBoost model necessitates only minor hyperparameter tuning, and its performance is relatively insensitive to the selection of hyperparameters (Gao and Ding, 2020; Barnwal et al., 2022).

Previous research indicates that numerous <u>featuresfactors</u> significantly impact hydrological drought.

Zou et al. (2018) demonstrated that climate change is the primary <u>factor feature</u> affecting hydrological drought on long-term scales. Wang et al. (2021) found that climatic variables such as precipitation and

evapotranspiration significantly influence the duration of hydrological drought. Additionally, Gan et al. (2023) revealed that large-scale climatic featuresfactors and sunspot activity have a substantial impact on hydrological drought events in the Huaihe River Basin. Despite many studies showing that machine learning models outperform physical models in terms of prediction accuracy, these models lack transparency and interpretability. Most research on machine learning models for drought prediction focuses on model performance, often neglecting the role of different featuresfactors influencing drought occurrence in model predictions. For example, Xu et al. (2022) established a hybrid model combining autoregressive integrated moving averages (ARIMA) and long short-term memory (LSTM) to predict the standardized precipitation evapotranspiration index at multiple time scales. Yu et al. (2023) combined the Hydrologiska Byrans Vattenbalansavdelning (HBV) model with an LSTM neural network to improve the prediction ability for semi-arid basins. Yalcin et al. (2023) proposed a hybrid model of convolutional neural networks (CNN) and LSTM to enhance the prediction accuracy of the standardized precipitation evapotranspiration index. However, these studies do not consider the influence of different featuresfactors on the model output.

Recent advancements in Explainable AI (XAI) techniques have provided opportunities for understanding why models make certain predictions (Gunning et al., 2019; Islam et al., 2022). Recently, local interpretability methods have been developed and can be implemented for neural network and random forest model architectures (Ribeiro et al., 2016a). The Local Interpretable Model-Agnostic Explanation (LIME) method has been widely used, but it exhibits a high degree of instability due to considerable variation in its explanations upon repeated use (Ribeiro et al., 2016b). Therefore, the Shapley Additive Explanations (SHAP) approach was proposed as a solution. Grounded in the strong theoretical basis of game theory, it provides more robust mathematical accuracy and consistent extension on top of the LIME framework (Lundberg and Lee, 2017; Molnar, 2022). At present, SHAP has been applied to a variety of prediction scenarios, there are few studies on interpretable machine learning using the SHAP algorithm. For example, Dikshit and Pradhan (2021) employed an LSTM model combined with the SHAP algorithm to predict droughts, demonstrating that the inclusion of climate variables as predictors can enhance prediction accuracy. Similarly, Mardian et al. (2023) utilized an XGBoost model and SHAP to forecast predict droughts in the Canadian prairies, and clarified the importance of spatial and temporal predictors, drought indicators, GRACE groundwater distribution and teleconnection in drought prediction. Similarly, Xue et al. (2024) analyzed the spatial and temporal characteristics and

driving factors of agricultural drought during the extreme drought period in northern Italy in 2022 by using the integrated machine learning model explained by SHAP combined with the new integrated agricultural drought index (IADI), quantified the dominant factors, and revealed that meteorological conditions were the main driving factors. Likewise, Zeng et al. (2025) used the XGBoost model explained by SHAP combined with the new rate of extension (RE) index to analyze the spatial and temporal evolution of meteorological drought characteristics in the Yangtze River Basin of China, quantified the dominant driving factors, and revealed that soil moisture was a primary factor. However, the range of drought-influencing featuresfactors considered in their research is still not comprehensive enough. For example, soil temperature and water content, surface thermal radiation and other featuresfactors are also important featuresfactors affecting drought (Raposo et al., 2023).

89

90

91

92

93

94

95

96

97

98

99

100

101

102

103

104

105106

107

108

109

110

111

112

113

114

In light of the above, the novelty of this study is to employ interpretable machine learning models for hydrological drought prediction and to identify the contribution of different influencing features factors to the model prediction results. While SPI is a precursor to SRI, this study disentangles the hierarchy of contributing featuresfactors, including SPI, large-scale climate indices, and soil moisture etc. Soil moisture directly affects hydrological drought, and it can analyze the contribution of different featuresfactors to drought when it is predicted together with drought featuresfactors such as large-scale climate features faetors. For example, Mardian et al. (2023) employed a method combining the XGBoost model with SHAP (Shapley Additive Explanations) values, utilizing a variety of drought-influencing featuresfactors such as large-scale climatic featuresfactors and soil moisture, to predict drought conditions in the context of the Canadian Drought Monitor (CDM) and to understand the underlying driving featuresfactors. Therefore, the objectives of the study are: i) Utilizing the XGBoost model, combined with 26 features factors predicted monthly and 18 features factors predicted seasonally, the hydrological drought in the Huaihe River Basin is predicted, and the performance evaluation is carried out by using precision and recall indicators; ii) Various SHAP plots were employed to gain insights into the model outputs and analyze the influence of different drought variables on the predictive results of the model.

2 Study area and data

2.1 Study area

115

116

117

118

119

120

121

122123

124

125

126

127

128 129

130 131

132

133

134

135

136

137

138

In this paper, as shown in Figure 1, the Huaihe River Basin is selected as the research area, and the grid is divided at a resolution of 1°lat×1°lon, with a total of 28 grid regions, which takes into account the computational feasibility and spatial heterogeneity. Although large-cale climatic features factors have spatial consistency, their effects on regional precipitation can be different through local terrainatmosphere feedback (Lu et al., 2006). Gridded analysis identifies sensitive subregions, supporting targeted mitigation. The Huaihe River Basin is located at 111°55'-121°25'E, 30°55'-36°36'N, covering an area of approximately 270,000 square kilometers. It experiences significant spatiotemporal variations in precipitation, with an average annual precipitation of around 883 millimeters. Situated in the transitional climatic zone from south to north, the southern part of the basin falls under a subtropical climate, while the northern part experiences a warm temperate climate. The average annual temperature ranges from 11 to 16°C. The winter and spring seasons in the basin are relatively dry, while the autumn and summer seasons are hot and rainy, resulting in pronounced seasonal fluctuations between droughts and floods. The average annual runoff depth in the basin is 230 millimeters. Due to its unique geographical location, the area is prone to frequent flooding, leading to high water levels and prolonged flood conditions. In addition, the annual average water surface evaporation in the Huaihe River Basin ranges from 900 to 1500 millimeters. As one of the important agricultural production bases in China, the basin is densely populated with substantial water demands. However, the region frequently suffers from drought disasters. Since the beginning of the 21st century, an average of 2.698 million hectares of crops, accounting for 21% of the total cultivated land area in the basin, have been affected annually. The Huaihe River Basin is a significant agricultural area and a high-population-intensive area in eastern China. Seasonal droughts frequently affect food production and water resources. One-month advance prediction is essential for reservoir scheduling, irrigation planning and early warning times for farmers.

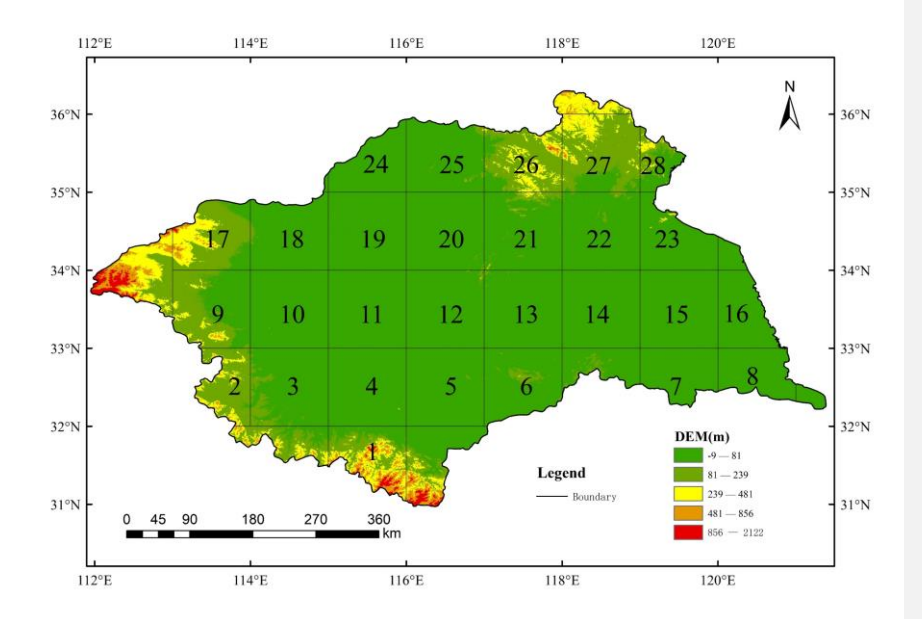


Figure 1: Huaihe River Basin and 28 grid area location.

2.2 Data

We obtained monthly average precipitation, wind speed, temperature, evapotranspiration, monthly average runoff, 0-10cm soil moisture, and 100-200cm soil moisture data sets for the Huaihe River Basin from the website https://disc.gsfc.nasa.gov/datasets/GLDAS_NOAH10_M_2.0/ for the period 1960 to 2014. The monthly average 2 m dewpoint temperature, surface net solar radiation, surface net thermal radiation, surface pressure, and leaf area index data sets were obtained from the ERA5-Land reanalysis dataset (https://cds.climate.copernicus.eu/). According to whether the grid center point falls within the basin, 28 grid regions are defined. If the center point of the grid is not within the basin boundary, the region is not divided into grids. The grid analysis is carried out with these grid points as the center and 1°lat×1°lon as the resolution, covering a total of 28 grid regions. Using the interpolation method based on the Xarray packageUsing the interpolation method in array, the data of Huaihe River Basin are interpolated to 28 grid regions.

Numerous studies have demonstrated the significant influence of large-scale climate indices, including the Atlantic Multidecadal Oscillation (AMO), Arctic Oscillation (AO), North Pacific pattern (NP), Pacific Decadal Oscillation (PDO), and Nino3.4, on drought dynamics(Gan et al., 2023; Phan-Van et al., 2022; Wu and Xu, 2020; Xiao et al., 2019). For example, the positive phase of AMO leads to a

decrease in summer precipitation in the Huaihe River Basin by enhancing the western Pacific subtropical high (Lu et al., 2006); the Pacific Decadal Oscillation (PDO) has the most significant impact on the monthly runoff in the Huaihe River Basin (Sun et al., 2018). These selected climate featuresfactors (Nino3.4, AMO, TPI, PDO, AO, TNI, and NP) for the Huaihe River basin analysis were acquired from National Oceanic and Atmospheric Administration (NOAA) climate (http://www.esrl.noaa.gov/psd/data/climateindices), covering the period from 1960 to 2014.

3 Methods

157

158

159

160 161

162

163

164

165

166

167

168

170

171

172

173

174

175

176

177 178

179 180

181

182

3.1 Drought indicesex

In this study, the standardized precipitation index (SPI) (McKee et al., 1993) is used to characterize meteorological drought. SPI is widely used for drought risk assessment and monitoring due to its ease of calculation and ability to work on multiple time scales. The calculation method of SPI is as follows:

$$f(x) = \frac{x^{\alpha - 1} e^{\frac{x}{\beta}}}{\beta^{\alpha} \Gamma(\alpha)}$$
 (1)

带格式的: 两端对齐

$$F(x) = \int_0^x f(x)dx$$
 (2)

Assuming that the precipitation series x at a certain time scale follows a stationary gamma distribution, where α and β are the scale and shape parameters ($\alpha > 0$, $\beta > 0$). The cumulative probability F(x) of each item is normalized to obtain the corresponding SPI.

The standardized runoff index (SRI) was first proposed by Shukla and Wood (2008) as an effective and accurate index for describing hydrological drought characteristics. It has been widely used in hydrological drought identification. SRI is also calculated by transforming the cumulative flow distribution of a given time scale into a standard normal distribution using equiprobability transformation, similar to the calculation method of SPI. The SPI/SRI classes are classified as shown in Table 1 (Li et al. 2024). In this study, drought is classified into four classes, namely, Normal (ND), Mild drought (D1), Moderate drought (D2), and Severe drought and Extreme drought (D3), according to Table 1. However, due to the limited number of extreme drought events, it posed an issue in training the model. Therefore, the classes of Severe drought and Extreme drought were merged into one.

Table 1: Drought elasscategory classification and corresponding SPI-values and SRI values.

SPI/SRI value	<u>ClassCategory</u>
SPI/SRI> 0	Normal (ND)
<u>-1.0≤0 SPI/SRI</u> to <u><0</u> -1.0	Mild (D1)
-1.5 <u><</u> SPI/SRI<-1.0 <u>-1.0 to -1.5</u>	Moderate (D2)
<u>-2.0≤SPI/SRI<-1.5</u> <u>-1.5 to -2.0</u>	Severe (D3)Normal
	Mild-
	Moderate
	Severe
<u>SPI/SRI<</u> ≤ -2.0	Extreme(D3)Extreme

3.2 Machine learning models

183

184

185 186

187

188

189

190

191

192

194

197

199

In this paper, the XGBoost model is used for multi-input single-output regression prediction problems to predict the hydrological drought in the Huaihe River Basin. The XGBoost model is an ensemble learning algorithm belonging to the Boosting algorithm category. It utilizes decision trees as its basic elements and implements a gradient-boosting algorithm to minimize loss when adding new models. XGBoost aims to improve the training speed and predictive performance of gradient-boosting decision trees. The foundational knowledge about the mechanism and implementation behind XGBoost can be found in the paper by Chen and Guestrin (2016). Assuming we have K base models denoted as $f_t(x) \in F$ t = 1,2,...,K, where F the model space contains all the base models, the XGBoost model can be represented using the following function:

Where the parameters of the XGBoost model primarily consist of the structure of each tree and the

195 scores in the leaf nodes, that is, the learning of each function $f_t(x)$

196 As each base model is generated in a certain sequential order, the creation of the subsequent tree-

takes into account the predictions made by the preceding tree. Therefore, the objective function of the -t

198 base model can be expressed as follows:

$$\underline{\qquad} y^{(t)} = \sum_{i=1}^{n} t \left(y_i, \hat{y}_i^{(t-1)} + f_t(x_i) \right) + \Omega(f_t)$$
(4)

带格式的: 正文,缩进:首行缩进: 0.74 厘米,行距: 1.5 倍行距

带格式的: 两端对齐,缩进:首行缩进: 0 字符

设置了格式:字体: (默认) Times New Roman

带格式的:缩进:首行缩进: 0 字符

带格式的: 正文,缩进:首行缩进: 0.74 厘米,行距: 1.5 倍行距

Here, $l(y_i, \hat{y}_i^{(t-1)})$ represents the loss function related to $y_i, \hat{y}_i^{(t-1)}$, $y_i^{(t-1)}$ denotes the 200 predictions of the first t-1 decision trees for sample \dot{t} (i.e., the sum of predictions made by the first 201 t-1-trees), y_i represents the actual value of sample \dot{t} -, $f_i(x_i)$ represents the prediction of the \dot{t} 202 decision tree for sample \dot{t} , and $\Omega(f_t)$ represents the model complexity of the \dot{t} tree. Therefore, 203 the predictions of the first k-trees for the sample i-are equal to the predictions of the first k-1204 205 trees plus the prediction of the k tree. 206 3.3 Modeling Settings Model input data The study period for this research spans from 1960 to 2014, with the model training period from 207 208 1960 to 2003 and the prediction period from 2004 to 2014. The input and output data types for 28 grid 209 areas are the same. We use a sliding window of 12 and 3 months. The prediction lead time is 1 month. The relevant settings for models modeling are shown in Table 2. 对图 2 的 Input Window Lead time 210 进行说明。 211

Take the 7th grid area as an example. When using monthly data, the input was 26 different drought influencing features, and the output was SRI-1. The number of input samples during model training was 13767, and the number of output samples was 526. There are 3432 input samples and 132 output samples during the model prediction period. When using seasonal data, the input is 18 features without drought, and the output is SRI-3 in different seasons. The number of input samples during model training is 792, and the number of output samples is 44. The number of input samples in the model prediction period is 198, and the number of output samples is 11. The model uses Bayesian hyperparameter optimization to find the optimal parameters, such as learning rate, tree depth, and number

220 221

222

212

213

214

215

216

217

218

219

Table 2. Model setup and data overview

of iterations. Table 2 gives the relevant settings of model modeling.

Phase	Data Period	Input Window	Forecast_	Ooutput •
			HorizonLead time	
Training phase	1960-2003	M-12 to M-1	1 months	SRI-1-
(monthly time		(12month)		<u>value</u>
scale)Monthly training set				

带格式的: 缩进: 首行缩进: 2 字符, 行距: 1.5 倍行距

设置了格式: 字体: (默认) Times New Roman, (中文) 宋体,小五,加粗

带格式的: 正文,段落间距段前: 0 磅,段后: 0 磅, 行距: 1.5 倍行距

设置了格式:字体:(中文) 宋体, 小五

带格式的:缩进:首行缩进: 0 字符

带格式的:居中

格式化表格

7H 24 FUACTH

带格式的:居中

Validation phase	2004-2014	M-12 to M-1	1 months	<u>SRI-1-</u> 设置了格式: 字体: 10 磅
(monthly time		(12month)		<u>value</u> ◆ 设置了格式: 字体: 10 磅
scale)Monthly Test Set				带格式的: 居中
Training phase	1960-2003	M-3 to M-1	1 months	<u>SRI-3</u> _
(seasonal time scale)		(3month)		value ◆ 带格式的: 居中
Seasonal scale training set				
Validation phase	2004-2014	M-3 to M-1	1 months	<u>SRI-3</u> _
(seasonal time		(3month)		walue ◆ 带格式的: 居中
scale)Seasonal scale				

The XGBoost model for 28 grid areas is established, and the data types used in each region are the same. As shown in Table 3+, for the monthly data analysis, 26 different drought-influencing features factors were considered. These include a month-scale SPI (SPI-1) and SPI indices at different time scales of 1 month and 2 months in advance. Large-scale climate indices (AMO, TPI, PDO, AO, TNI, NP), evapotranspiration, wind speed, 2 m dewpoint temperature, soil moisture content, surface net thermal radiation, surface net solar radiation, surface pressure and leaf area index were considered.

prediction set

As shown in Table 23, for seasonal data analysis, the basin data are classified by season, and 18 different drought influencing <u>featuresfactors</u> are used. It includes SPI-3 value, soil moisture content, evapotranspiration, surface net thermal radiation, air temperature, NINO3.4, NP, wind speed, TNI, PDO, TPI, surface pressure, AO, AMO, leaf area index, 2 m dewpoint temperature and surface net solar radiation in four seasons.

For monthly and seasonal data sets, SHAP (Shapley Additive Explanation) values were used to analyze the contribution of 28 grid regions to determine the impact of each <u>featurefactor</u>.

Monthly-scale predictions capture the rapid onset of drought, which is critical for early warning systems, whereas seasonal analysis aligns with agricultural planning cycles. Thus, our study employs both monthly and seasonal analyses to comprehensively assess short-term variability and long-term trends in hydrological drought.

Table 23: The monthly scale and seasonal scale of the model predict the input target variables. The drought impact factors of the monthly scale prediction input of the model (T is the lead time, SPI-1, SPI-3, SPI-6, and SPI-9 are SPI values at different monthly scales.).

SPI-1, T=1 SPI-1, T=1 SPI-3, T=1 SPI-6, T=1 SPI-9, T=2 SPI-1, T=2

SPI-3, T=2 SPI-6, T=2 SPI-9, d2m temperature, surface pressure,

Prought influencing
features (monthly)

evapotranspiration, Air temperature, wind speed, surface net solar

radiation, surface net thermal radiation, 0-10cm soil moisture, 100-200cm

soil moisture, Nino3.4, AMO, PDO, AO, TNI, NP, TPI, leaf area index

SPI-3 (different seasons), d2m temperature, surface pressure,

<u>Prought influencing</u> evapotranspiration, Air temperature, wind speed, surface net solar

<u>feature (seasonal)</u>

<u>radiation, surface net thermal radiation, 0-10cm soil moisture, 100-200cm</u>

soil moisture, Nino3.4, AMO, PDO, AO, TNI, NP, TPI, leaf area index

Drought influencing factors (monthly)

243

Ü	U	,
+		SPI-1
2		T=1 SPI-1
3		T=1 SPI 3
4		T=1 SPI 6
5		T=1 SPI-9
6		T=2 SPI-1
7		T=2 SPI 3
8		T=2 SPI-6

带格式的: 居中,段落间距段前: 5 磅,段后: 5 磅, 行距: 2 倍行距

设置了格式:字体:10磅,非加粗

设置了格式: 字体: 10 磅

带格式的: 居中 格式化表格

设置了格式:字体:10磅,非加粗

设置了格式:字体:10磅,非加粗

带格式的: 居中,段落间距段前: 5 磅,段后: 5 磅, 行距: 2 倍行距

设置了格式: 字体: 10 磅

带格式的:居中 **设置了格式:**字体:10磅

设置了格式: 字体: 10 磅, 非加粗

及直1作26. 1 件. 10 奶, 17加加

	9	T=2 SPI-9
-	10	d2m temperature
÷	11	surface pressure
=	12	evapotranspiration
-	13	Air temperature
=	14	wind-speed
-	15	surface net solar radiation
÷	16	surface net thermal radiation
-	17	0-10cm soil moisture
÷	18	100-200em soil moisture
=	19	Nino3.4
4	20	AMO
ź	21	PDO
(22	AO
ź	23	TNI
í	24	NP
á	25	TPI
í	26	leaf area index

244 Table 3: The drought impact factors of seasonal prediction input of model.

Drought influencing factors (seasonal)

4	SPI-3 (different seasons)
2	d2m temperature
3	surface pressure
4	evapotranspiration
5	Air temperature
6	wind-speed
7	surface net solar radiation
8	surface net thermal radiation
9	0-10em soil moisture
10	100-200cm-soil moisture
#	Nino3.4
12	AMO
13	PDO
14	A O
15	TNI
16	NP
17	TPI

18 leaf area index

3.4 Model evaluation

Based on the optimal parameters obtained during the training phase, the XGBoost model is utilized to predict the hydrological drought situation in the Huaihe River Basin from 2004 to 2014. These predictions will be assessed using precision, recall, and the Heidke Skill Score (HSS) as measurement metrics. Precision is defined as the ratio of correctly classified instances of a specific elasscategory to the total number of predicted instances, quantifying the model's precision in predicting drought conditions and evaluating its reliability. Conversely, Recall represents the ratio of correctly classified instances of a specific elasscategory to the total number of observed instances in that elasscategory, capturing the probability of the model predicting observed drought conditions and reflecting its sensitivity (Mardian et al., 2023; Zhang et al., 2023). The Heidke Skill Score (HSS) measures the model's classification performance relative to random chance, accounting for both correct and incorrect predictions. It is particularly useful for assessing predictive skill in imbalanced datasets (Heidke, 1926). The following are the precision, recall and HSS formulas:

$$precision = \frac{TP}{TP + FP}$$
 (15)

$$Recall = \frac{TP}{TP + FN} \tag{26}$$

261
$$HSS = \frac{2 \times (TP \times TN - FN \times FP)}{\left[(TP + FN) \times (FN + TN) + (TP + FP) \times (FP + TN) \right]}$$
(3)

Where the classification evaluation metrics employed are True Positives (TP), <u>True Negative (TN)</u>. False Positives (FP), and False Negatives (FN). TP denotes the number of actual positive samples correctly predicted as positive, <u>TN is the actual number of negative samples that are correctly predicted to be negative</u>, FP represents the number of actual negative samples incorrectly predicted as positive, and FN signifies the number of actual positive samples incorrectly predicted as negative.

3.5 Shapley Additive Explanations (SHAP)

SHAP, a machine learning interpretability method, provides a unified approach by combining elements from additional variable attribution methods with Shapley values as a measure of variable

域代码已更改

设置了格式:字体:非倾斜

importance. Shapley values were originally introduced in game theory to determine the contributions made by each player in cooperative games. The fundamental idea is that each player receives a corresponding payout based on their contribution (Shapley, 1953). The interpretation of SHAP values is straightforward: larger absolute SHAP values indicate greater weight of the variable in predicting the model, while negative (positive) SHAP values exert a negative (positive) influence on the prediction process. Lundberg and Lee (2017) developed the SHAP method based on the theoretical foundation of Shapley values to explain the influence of each variable on model predictions, thereby providing increased transparency to the model. The Shapley value is calculated as the average marginal contribution based on all possible variable permutations. Importantly, SHAP values reflect local feature importance, meaning that they quantify the contribution of each variable to a specific prediction instance, rather than summarizing its overall effect across the entire dataset. The mathematical expression for the classic SHAP value is as follows:

带格式的: 正文, 缩进: 首行缩进: 2 字符, 行距:

$$\varphi_{i} = \sum_{S \subseteq N} \frac{|S|!(n-|S|-1)!}{n!} \Big[\nu \big(S \cup \{i\} \big) - \nu \big(S \big) \Big]$$
 (7)

Where φ_i represents the contribution of variable \dot{t} , N represent the set of all variables, n denote the number of variables N, S indicate the subset of N that includes variable \dot{t} , and v(N) represent the baseline, which signifies the predicted outcome of each variable in N when their values are unknown.

The model results for each observed value are estimated by summing the SHAP values of each variable corresponding to that observed value. Hence, formulating the explanation model as follows:

289
$$\frac{g(z') = \phi_0 + \sum_{i=1}^{M} \phi_i z'_i}{-(8)}$$

Where, $Z' \in \{0,1\}^M$, the variable quantity is denoted as M, and the value ϕ_i can be obtained from equation (7). SHAP offers a variety of AI model explainers.

带格式的: 正文, 缩进: 首行缩进: 2 字符, 行距: 1.5 倍行距

In this study, we utilized a tree explainer to compute SHAP values based on the best XGBoost model for assessing drought impacts, aiming to estimate the contributions of each variable. In our study, the SHAP baseline is the difference between the prediction of the model and the average prediction on the data set. For each sample and each feature, the SHAP value is the difference between the predicted value of the model containing the feature and the predicted value after removing the feature and the baseline. We use these SHAP values to quantitatively analyze the positive or negative effects of each predictor on hydrological drought prediction.

299

300

301

302

303 304

305

306

307

308

309

310

311

312

313

314

315

316

317

318

319

320

321

292 293

294

295

296

297

298

4 Results

4.1 Model performance

The study period for this research spans from 1960 to 2014, with the model training period from 1960 to 2003 and the prediction period from 2004 to 2014. The input and output data types for 28 grid areas are the same. Take the 7th grid area as an example, when using monthly data, the input was 26 different drought influencing factors, and the output was SRI-1. The number of input samples during model training was 13767, and the number of output samples was 526. There are 3432 input samples and 132 output samples during the model prediction period. When using seasonal data, the input is 18 factors without drought, and the output is SRI-3 in different seasons. The number of input samples during model training is 792, and the number of output samples is 44. The number of input samples in the model prediction period is 198, and the number of output samples is 11. According to the data in Table 44 and Figure 2, the overall precision of the XGBoost model is 79.9%, which means that it has a 79.9% ability to correctly identify drought elassescategories. In the identification of the ND drought elasscategory, the performance of the model is particularly excellent. Figure 2 shows that the median precision and recall rate of the ND elasscategory areis both more than 0.8. It can be seen from the data in Table 4 that the recall rate of the ND drought elasscategory is 91% and the precision rate is 88%, which proves that the model has high sensitivity and reliability in predicting the ND drought elasscategory. For ND, the HSS is 0.77, showing a significant discriminant advantage over the no-skill baseline that always predicts the most common category. At the same time, the precision rates of ND and D3 drought classescategories are 88% and 86%, respectively, indicating that the model had good prediction accuracy for these two types of droughts. However, the precision rates of the D1 and D2 drought elassescategories are 74% and 61%, respectively, reflecting the lack of prediction accuracy of the model in these elassescategories.

批注[李敏1]:需要核对表的序号

In addition, the boxplot in Figure 2 further reveals the precision and recall performance of the model for each drought elasscategory in 28 grid regions. Although the median precision and recall of the D1 drought elasscategory areis both close to 0.8, indicating that the model has a high predictive ability in this elasscategory, the performance of the D2 and D3 drought elassescategories is relatively poor. Especially for the D3 drought elasscategory, the median recall rate does not exceed 0.5, indicating that the model is not sensitive to the identification of such drought events, and there are some limitations in the prediction. However, although the recall rate of the D3 drought elasscategory is low, its precision is almost as high as the ND drought elasscategory, which is mainly due to the low frequency of D3 drought elasscategory events. The model can successfully capture all D3 drought elasscategory events in some grid areas, thereby improving the precision of this elasscategory. The HSS metric complements precision and recall by evaluating the model's performance relative to the no-skill baseline, with Vvalues closer to 1 indicateing superior performance. The declining HSS from ND to D2 underscores the model's reduced discriminatory power for less extreme drought categories, aligning with the observed precision-recall trade-offs.

Table 44: The average accuracy, recall and HSS of each drought category in 28 regional models. The average accuracy and recall rate indicators for each drought level predicted by the 28 regional models.

Category	Precision (%)	Recall (%)	HSSes
<u>ND</u>	<u>88</u>	<u>91</u>	0.77
<u>D1</u>	<u>74</u>	<u>78</u>	0.61
<u>D2</u>	<u>61</u>	<u>47</u>	0.46
<u>D3</u>	<u>86</u>	<u>50</u>	0.59
Average	<u>77.3</u>	66.5	0.608

220

Class	Precision (%)	Recall (%)
ND	88	91
D1	74	78
D2	61	47
D3	86	50

设置了格式 :字体: 非加粗	
格式化表格	
设置了格式 :字体:非加粗	
带格式的 :居中	
设置了格式 :字体:非加粗	
设置了格式: 字体:非加粗	
带格式的 :居中	
设置了格式: 字体:非加粗	
设置了格式: 字体:非加粗	
带格式的 :居中	
设置了格式:字体:非加粗	
设置了格式:字体:非加粗	
带格式的 :居中	
设置了格式:字体:非加粗	
格式化表格	

带格式的: 居中

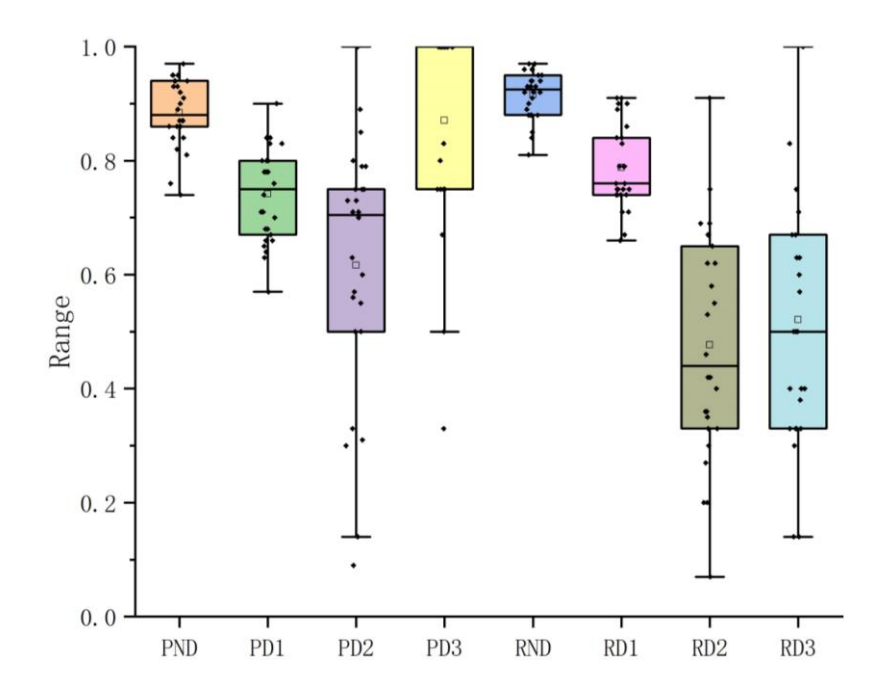
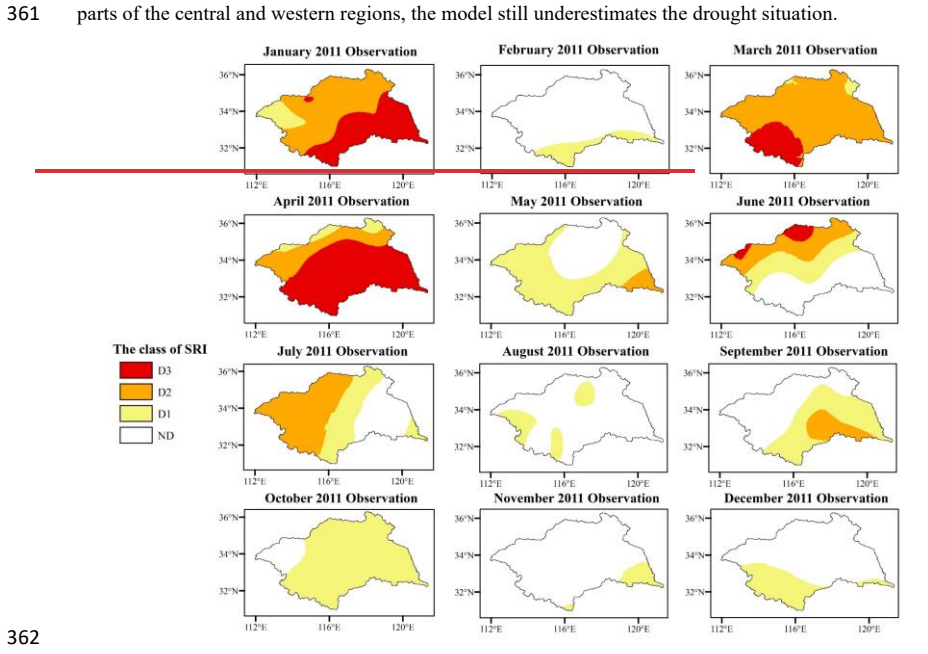


Figure 2: Box plots of the accuracy and recall rates of the four drought categories predicted by the 28 regional models ('P' represents the accuracy rate, and 'R' represents the recall rate. The small square represents the average.).

4.2 Prediction maps

According to the predicted drought data, 2011 was identified as a year with relatively severe drought conditions. To visually assess the predictive capability of the model, drought predicted, observed, and difference maps were created for each month of 2011 (Figure 3 to Figure 54). Figure 3 shows the comparison between the prediction and observation in the first six months of 2011, and the complete month map is placed in the appendix. In 2011, the model accurately captured drought situations across most regions. In January, the drought situation was severe, and the drought elasscategory was mainly in the D2 and D3 elassescategories. However, the prediction map of the model shows that the drought degree in most regions is lighter than the actual drought situation, and the drought elasscategory is mainly classified as D1, which relatively underestimates the actual situation of drought. In February, the drought situation was rapidly reduced, and the prediction map of the model was basically consistent with the observation map. In March and April, the drought conditions in the entire basin rapidly escalated and

became severe, and most of the areas in the observation map reached the drought elassescategories of D2 and D3, and only a few areas in the north were classified as D1 drought elasscategory. Consequently, this period poses a considerable challenge to the predictive ability of the model, making it an appropriate period to evaluate the predictive performance of the model. In general, the model effectively predicts the occurrence and deterioration of drought and captures the spatial distribution pattern. However, in some parts of the central and western regions, the model still underestimates the drought situation.



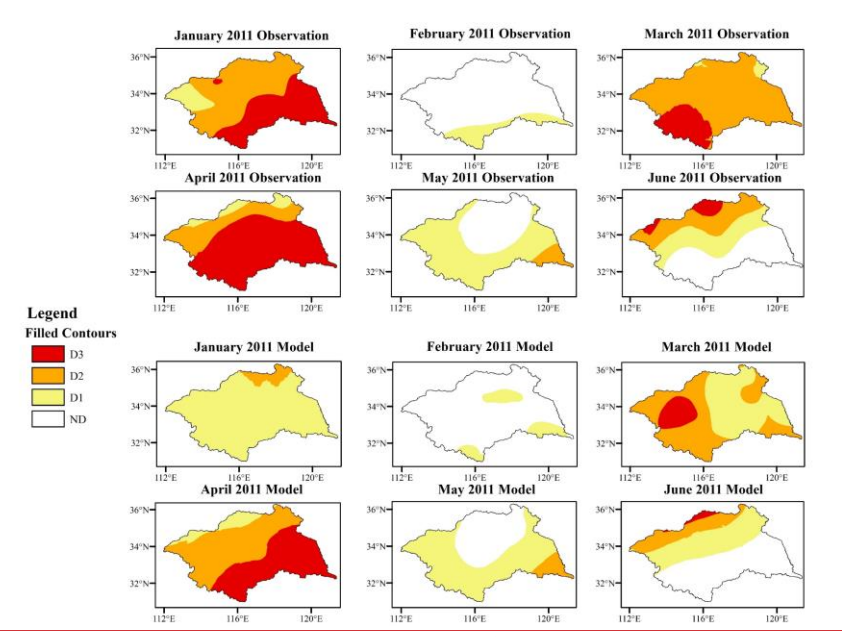


Figure 3: Monthly model predictions and observed drought categories for the first six months of 2011 The observed drought types of each month in 2011.

In May, the severity of the drought situation decreased relative to the previous two months, and the actual observed map and the model-predicted map were largely consistent. According to the observed map, in June, a drought occurrence was observed in the northern region where no drought had been previously recorded. Furthermore, in July, the drought area shifted from the northern to the western region. It was not until August that drought gradually diminished in most areas. Basically, the model captures the change of drought, but for some areas of D3 drought elasscategory, the model predicts them as D2 drought elasscategory.

批注[李敏2]: 观测值放到前面,观测值与模拟图最好中间镉一行或者半行

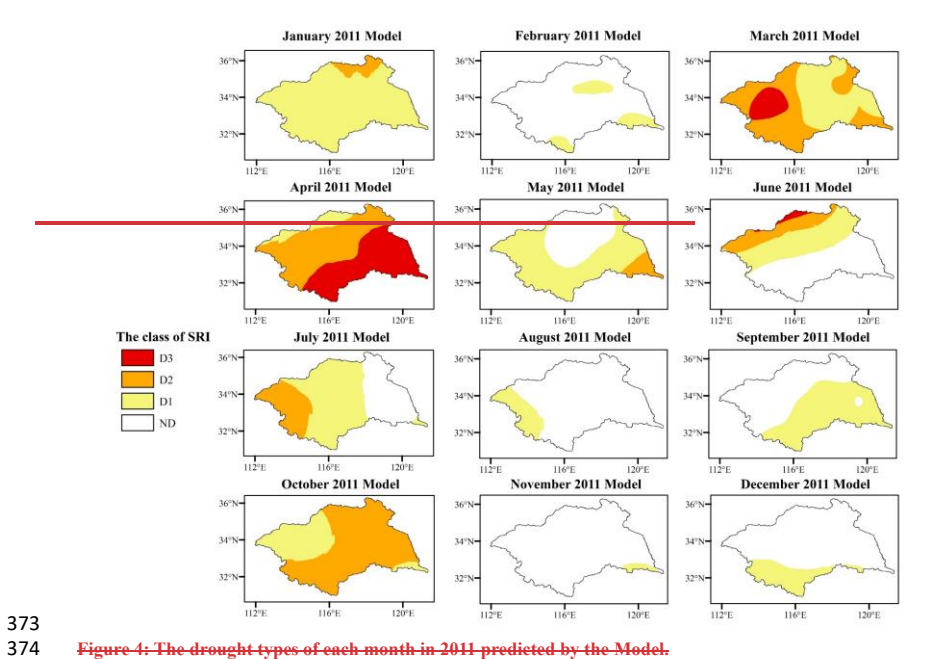


Figure 4: The drought types of each month in 2011 predicted by the Model.

375

376

377

378

379

380

381

382

In September, drought conditions were found in the eastern and southern regions on the observed map. However, the drought situation in some areas is underestimated on the map predicted by the model. In October, the model significantly overestimated the severity of the drought situation. According to the observed map, all regions except a small part of the western region experienced the D1 drought classcategory. In contrast, the model-predicted map shows widespread drought across the region, with most of the regions classified in the D2 drought elasscategory. In November and December, the drought in the observation map dissipated rapidly, and the drought situation was basically the same as that in the model prediction map.

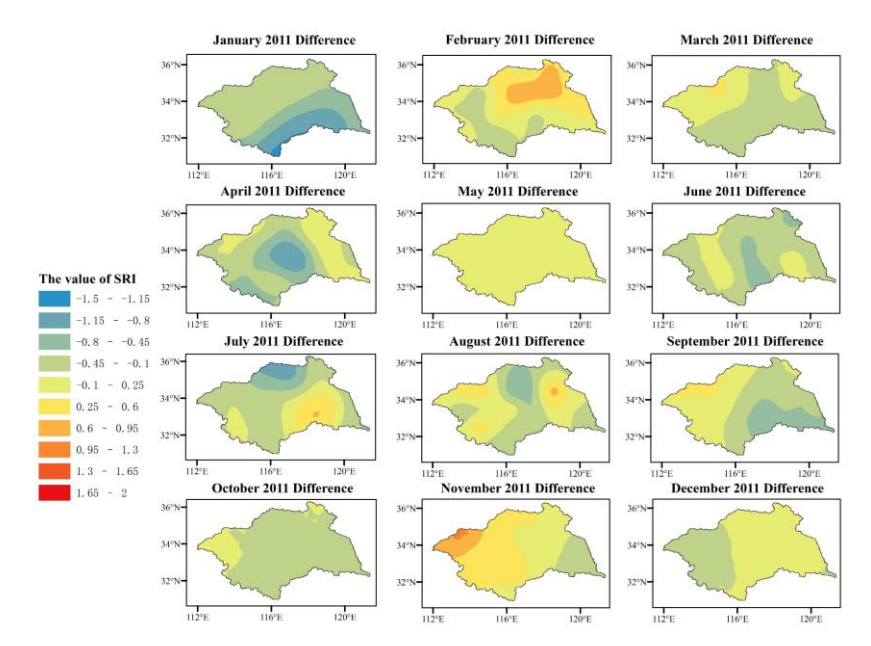


Figure 45: The difference between the predicted results of the model and the observed data values (Difference = SRI-prediction — SRI-actual) From blue to red indicates that the model predicts the degree of underestimation to overestimation of observations.

In general, the XGBoost model has a great performance in capturing the spatial structure and temporal dynamics of drought events during the 12-month period of 2011. However, the model indicates that while the model can distinguish between drought and non-drought conditions, it lacks clarity in defining the boundaries between different drought elassescategories. In most cases, the model underestimates drought conditions compared to the observed results.

4.3 Variable importance analysis

4.3.1 Monthly prediction analysis

To study the effects of different <u>featuresfactors</u> on drought, 26 different drought influencing <u>featuresfactors</u> were considered, and the corresponding influencing <u>featuresfactors</u> are analyzed for 28 grid regions, and the contribution analysis is made with SHAP values. Due to the limited space, only the analysis of the 7th grid region is shown in Figure 65. Figure 6-5 reveals the contribution of each input feature based on the SHAP value of each instance in 28 grid regions. In the vertical direction, the variables in the beeswarm plot are sorted according to their absolute SHAP values, which also reflects the importance of ranking variables. The density of points represents the eigenvalues of each instance in

each row. The X-axis shows the SHAP value corresponding to a single instance. The left side of the Y-axis of the bee colony graph represents the negative total contribution of the features in the XGBoost model, while the right side represents the positive total contribution. The negative and positive SHAP values represent the corresponding negative and positive total contributions of the related target variables the features to the total contributions of the related target variables the features to the total contributions of the related target variables the features to the total contributions of the related target variables the features. The larger the absolute value of SHAP is, the greater the contribution to the model is. The analysis reveals that SPI plays a dominant role, followed by AMO and evapotranspiration.

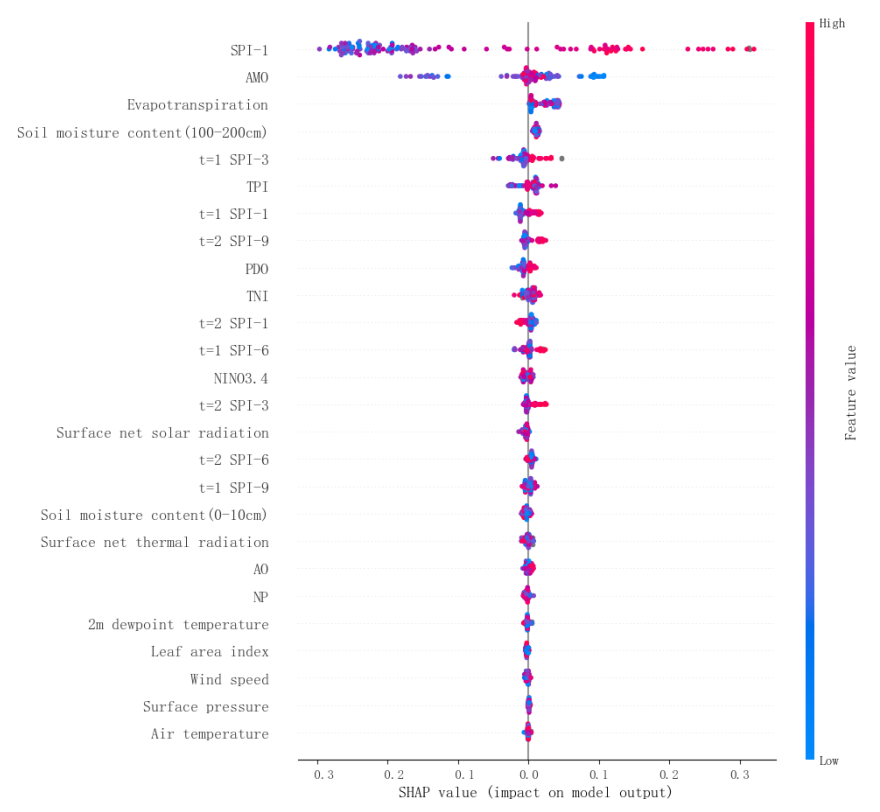


Figure 56: The SHAP values of 26 different influencing <u>featuresfactors</u> in each month of the 7th grid region from 2004 to 2014.

Figure 7 illustrates the interpretability of the XGBoost model focusing on the 7th grid region, providing insights into the average impact of the 26 influencing factors on model output. These findings corroborate the insights from Figure 6, highlighting that SPI, AMO, and evapotranspiration are the

√ 设置了格式:字体:加粗

predominant factors influencing the predictions of the model. Table 3 indicates that the absolute average SHAP value of SPI, incorporating monthly precipitation data for the entire basin, is 0.190, marking it as

417 the most substantial influence on hydrological drought within the 7th grid region.

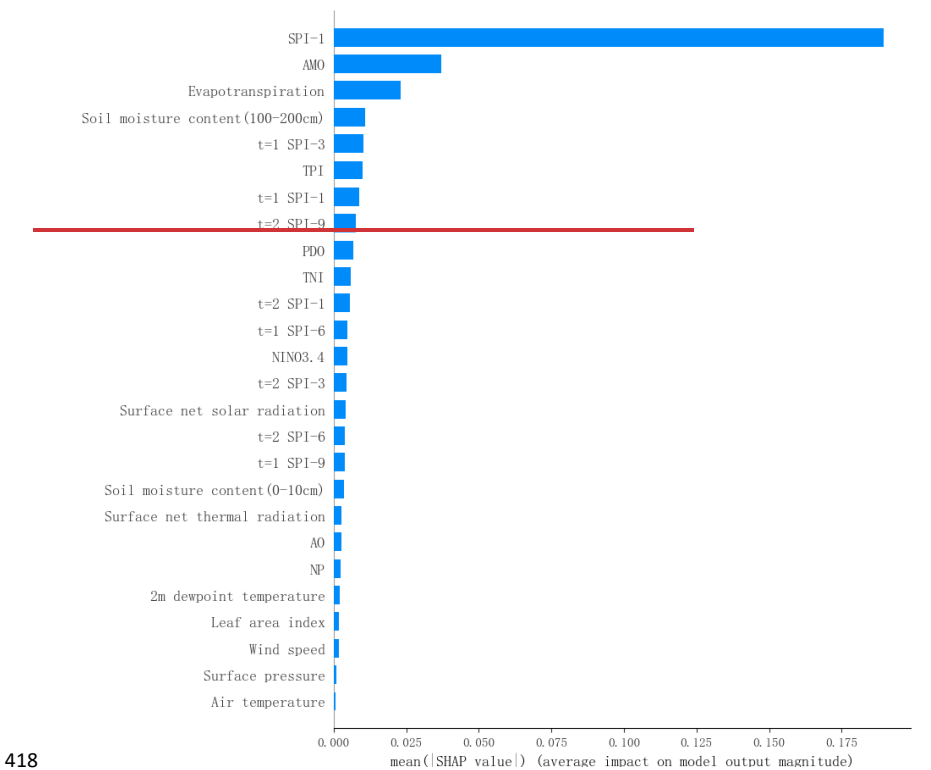


Figure 7: The absolute average SHAP values of 26 different influencing factors at the 7th grid region from 2004 to 2014.

To gain a deeper understanding of the <u>featuresfactors</u> contributing to drought events in the study area, As shown in Figure <u>68</u>, this study shows the spatial distribution of the first three main drought-influencing <u>featuresfactors</u> and discusses the changes of drought-influencing <u>featuresfactors</u> in the basin. The results show that the main influencing <u>factorfeature</u> of hydrological drought in the Huaihe River Basin is meteorological drought. As shown in Table <u>55</u>, the absolute average SHAP value of the first influencing <u>factorfeature</u> is significantly higher than that of the second and third influencing <u>featuresfactors</u>. Large-scale climate <u>featuresfactors</u> (particularly AMO) emerge as the secondary major influence, and about half of the North Central Basin is significantly dependent on these <u>featuresfactors</u>. For the third influencing <u>featurefactors</u>, a diverse range of large-scale climate variables, such as TPI, PDO,

NP, TNI, and AMO, affect almost half of the study area. In summary, the foremost determinant of hydrological drought is meteorological drought. Large-scale climate <u>featuresfactors</u> (notably AMO) rank second in importance, followed by <u>featuresfactors</u> like soil moisture content, and so on.

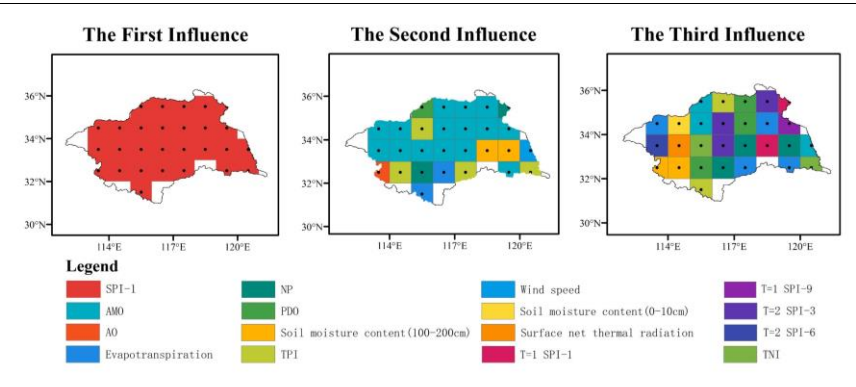
The findings demonstrate that the Standardized Precipitation Index (SPI) serves as the dominant driver of hydrological drought in the Huaihe River Basin, consistent with the conclusions of Gan et al. (2023), who identified meteorological drought as a critical precursor to hydrological extremes in this region. Further support arises from Wang et al. (2021), whose analysis of drought propagation mechanisms in the Huaihe Basin revealed indirect hydrological drought impacts mediated through soil moisture and evapotranspiration—a pattern corroborated by the secondary influence of soil moisture and evapotranspiration in this study. However, compared with the study of Zou et al. (2018) in the Weihe River Basin, the influence of large-scale climate <u>featuresfactors</u> in this study is more prominent, which may be related to the fact that the Huaihe River Basin is located in the climate transition zone and is more sensitive to the air-sea coupling phenomenon.

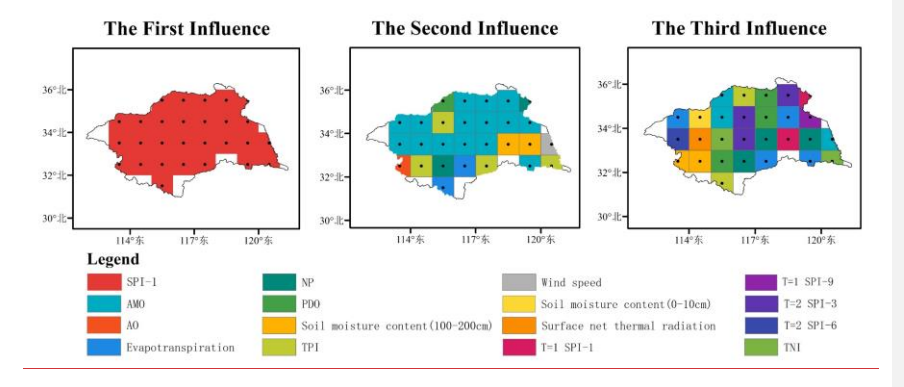
Table 55: The first three drought influencing <u>featuresfactors</u> and the SHAP value of the absolute average influence of 28 grid areas in Huaihe River Basin.

SHAP value Ggrid area	The first influencing factorfeatu re	Average SHAP value	The second influencing factor feature	Average SHAP value	The third influencing factor feature	Average SHAP value
1	SPI-1	0.160	Evapotranspiration	0.040	TPI	0.038
2	SPI-1	0.190	AO	0.018	Soil moisture content(100- 200cm)	0.014
3	SPI-1	0.189	TPI	0.030	Soil moisture content(100- 200cm)	0.023
4	SPI-1	0.178	NP	0.020	PDO	0.016
5	SPI-1	0.147	Evapotranspiration	0.044	NP	0.017
6	SPI-1	0.180	TPI	0.025	Evapotranspiration	0.021
7	SPI-1	0.190	AMO	0.037	Evapotranspiration	0.023
8	SPI-1	0.212	TPI	0.030	TNI	0.020
9	SPI-1	0.161	AMO	0.034	T=2 SPI-6	0.028
10	SPI-1	0.195	AMO	0.037	Surface net thermal radiation	0.031
11	SPI-1	0.226	AMO	0.037	TNI	0.012

→ 设置了格式:字体:加粗

12	SPI-1	0.221	AMO	0.033	T=2 SPI-3	0.017
13	SPI-1	0.228	AMO	0.028	NP	0.026
14	SPI-1	0.204	Soil moisture content(100-200cm)	0.057	T=1 SPI-1	0.029
15	SPI-1	0.160	Soil moisture content(100-200cm)	0.033	NP	0.032
16	SPI-1	0.157	Wind speed	0.033	AMO	0.030
17	SPI-1	0.186	AMO	0.064	Evapotranspiration	0.025
18	SPI-1	0.235	AMO	0.040	Soil moisture content(0-10cm)	0.032
19	SPI-1	0.168	TPI	0.055	AMO	0.035
20	SPI-1	0.172	AMO	0.038	T=2 SPI-3	0.026
21	SPI-1	0.165	AMO	0.039	PDO	0.039
22	SPI-1	0.179	AMO	0.042	Evapotranspiration	0.025
23	SPI-1	0.176	AMO	0.029	T=1 SPI-9	0.022
24	SPI-1	0.189	PDO	0.053	AMO	0.021
25	SPI-1	0.149	AMO	0.055	TPI	0.024
26	SPI-1	0.160	AMO	0.043	PDO	0.030
27	SPI-1	0.169	AMO	0.047	T=2 SPI-3	0.018
28	SPI-1	0.287	NP	0.025	T=1 SPI-1	0.016





设置了格式:字体:加粗

4.3.2 Seasonal prediction analysis

 To accurately reflect the differences in drought-influencing <u>featuresfactors</u> across different seasons, this study utilized 18 different drought-influencing <u>featuresfactors</u> to predict the hydrological drought in the Huaihe River Basin. Histograms of the absolute average SHAP values for different influencing <u>featuresfactors</u> in four seasons in the 7th grid region are presented in Figure <u>79</u>. The absolute average SHAP values of SPI-3 in spring, summer, autumn, and winter were 0.360, 0.261, 0.169, and 0.247 respectively, which had the greatest impact on hydrological drought in the same season. In addition, the absolute average SHAP values of evapotranspiration, soil moisture content, air temperature, and surface net thermal radiation were close to or exceeded 0.05, which also had a significant impact on hydrological drought in the Huaihe River Basin.

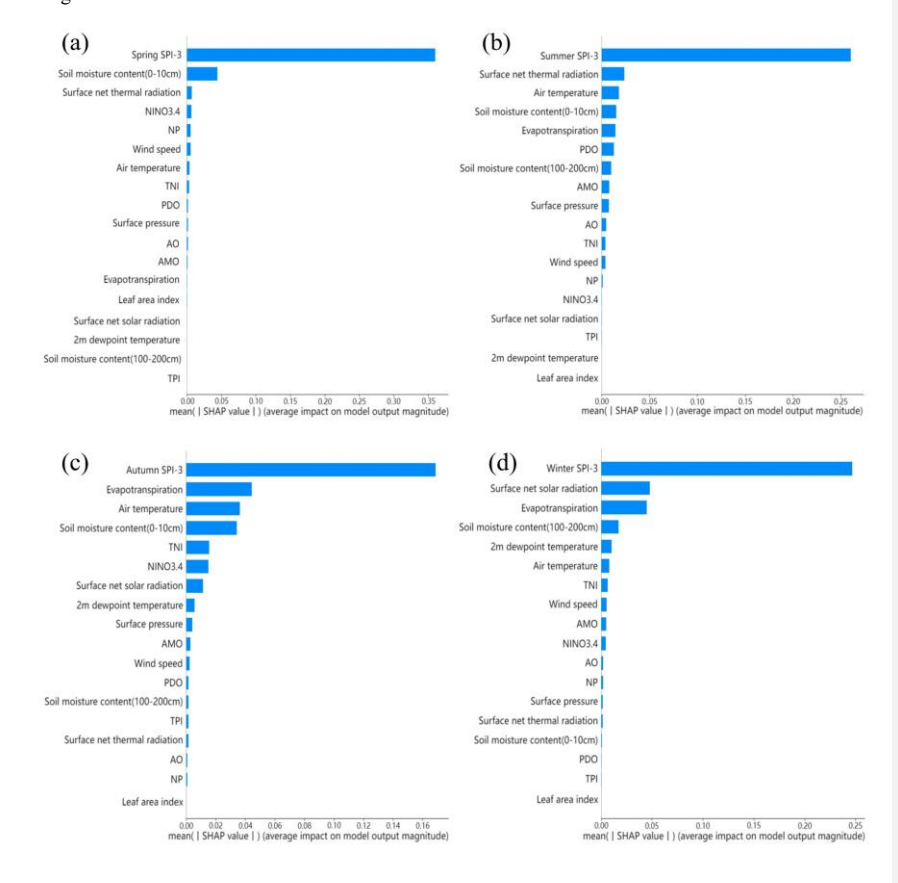


Figure 79: The absolute average SHAP values of 18 different influencing <u>featuresfactors</u> in the 7th grid region of four seasons ((a) Spring; (b) Summer; (c) Autumn; (d) Winter).

To understand the spatial and temporal distribution characteristics of drought and the potential

459

460

461

462 463

464

465

466 467

468

469 470

471

472

473

474

475

476

477

478

479

480

481

482

483

484

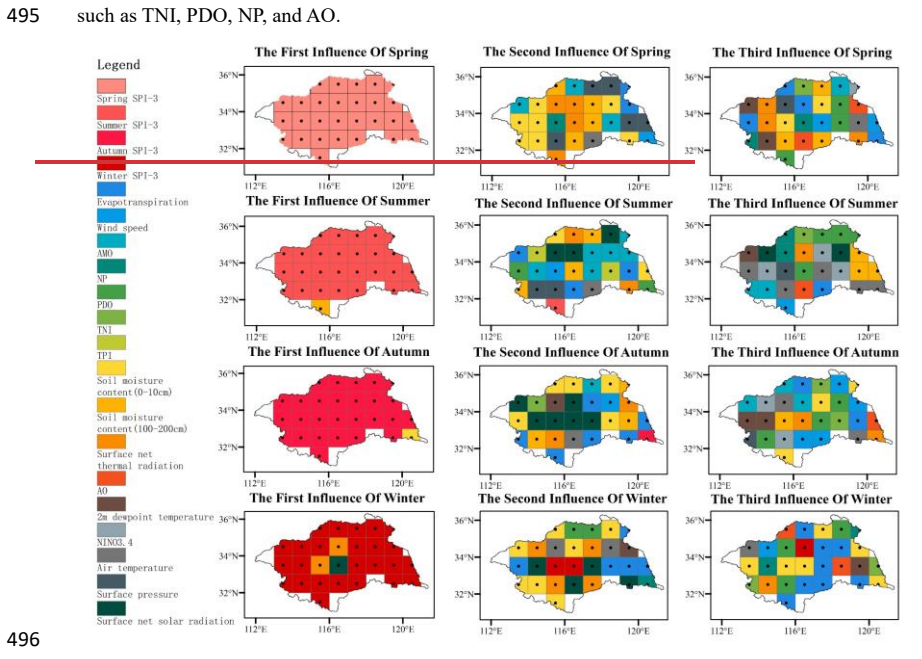
485 486

487

488

impact mechanism, Figure 810 displays the spatial distribution of the top three influencing featuresfactors in each season. The leading influencing featuresfactors across the four seasons include SPI-3, soil moisture content, and surface net thermal radiation, with SPI-3 being predominant across all seasons and regions. As shown in Figure 419, the absolute average SHAP value of the primary factorfeature exceeded the sum SHAP values of the second and third featuresfactors. Aside from SPI-3, soil moisture content also exerts a significant influence on hydrological drought in summer and autumn, particularly in the southern and southeastern parts of the river basin. In winter, certain areas in the central part of the river basin are mainly affected by surface net thermal radiation and surface net solar radiation. From the perspective of the second influencing factor feature, hydrological drought in most areas of the basin in spring is mainly affected by soil water content and evapotranspiration. In the rest of the region, surface pressure, temperature, radiation, and other features factors also play an important role. It is worth noting that in the 15th grid region, the surface pressure becomes a key secondary influencing factor feature, and its absolute average SHAP value reaches 0.175. This value is significantly higher than the second impact factor feature in other regions, and even close to the primary impact factor feature in the same grid area. This indicates that it is extremely sensitive to surface pressure in this particular place. During summer, the influence of large-scale climatic featuresfactors such as the AMO, PDO, and TPI becomes more pronounced compared to spring. Additionally, soil moisture content and surface radiation continue to account for a substantial proportion of the influence on hydrological drought. Regions with absolute average SHAP values surpassing 0.1 in summer constitute approximately one-seventh of the study area, indicating elevated sensitivity to these featuresfactors during this season. Similar to spring, soil moisture content and evapotranspiration remain predominant influencing features factors for hydrological drought in half of the grid areas during autumn and winter. The remaining regions are mainly influenced by surface net thermal radiation and surface net solar radiation. Specifically, during winter, the second influencing features factors for three grid regions (the 12th, 13th, and 21st grid regions) in the central part of the basin are soil moisture content and evapotranspiration, with absolute average SHAP values exceeding 0.1. This indicates a relatively higher influence of these secondary features factors in these regions compared to others.

Compared with the second impact factor feature, the large-scale climatic features factors in the third impact factor feature have an increased influence on hydrological drought in the four seasons. In spring and autumn, soil moisture content exhibits a more substantial influence on hydrological drought, while in summer, air temperature is considered to be a more important factor feature. However, in winter, half of the study areas continue to be dominated by soil moisture content and evapotranspiration, whereas most of the remaining study areas are primarily influenced by large-scale climate features factors features such as TNI, PDO, NP, and AO.



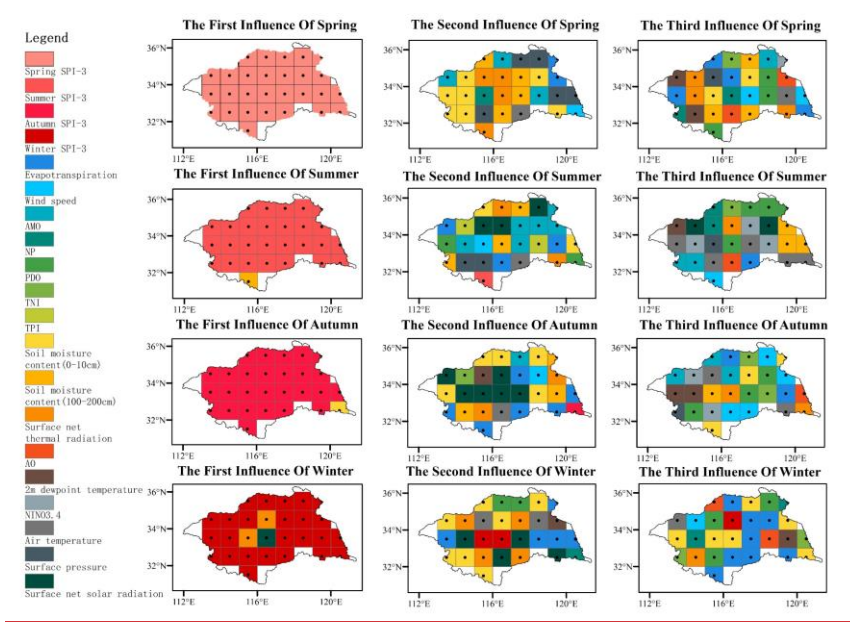
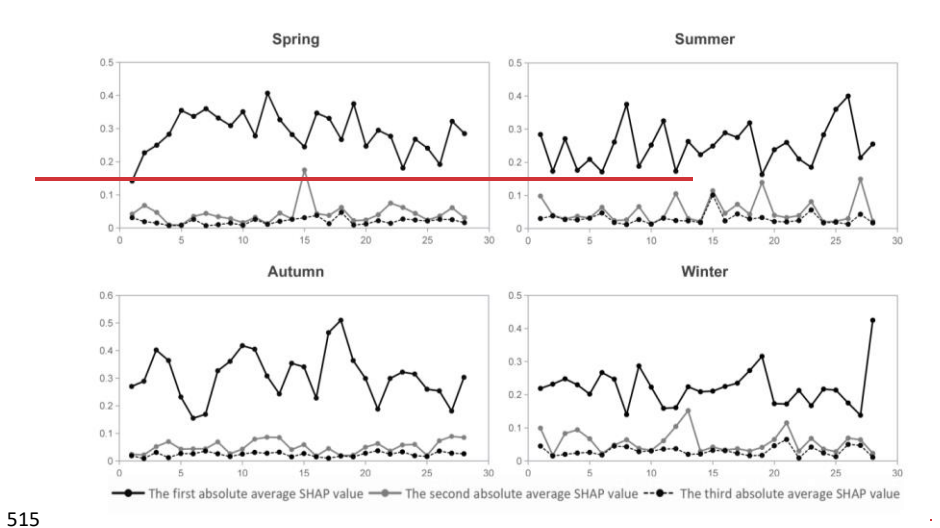


Figure 810: The first three drought-influencing factors features of 28 grid points in Huaihe River Basin in each season.

According to the above results, there were significant differences in the influencing factors features of drought among the four seasons. This diversity highlights the need for us to pay more attention to the weights and dynamic changes of various influencing factors features when predicting and understanding the spatial-temporal distribution characteristics of drought. Although the SPI factor feature continues to dominate, at some grid points, factors features such as soil moisture content in summer and autumn, as well as thermal radiation in winter, cannot be ignored. This suggests that even for the same influencing factor feature, its influence can vary greatly in different seasons and regions. Furthermore, in addition to the influence of meteorological drought, the influencing factors features of spring hydrological drought are mainly biased toward soil moisture content and evapotranspiration, in addition to surface pressure, temperature, radiation, and other related factors features. The absolute average SHAP value of these influencing factors features is basically no more than 0.1, which is very different from SPI-3, but its impact on hydrological drought cannot be ignored. In autumn and winter, the above factors features still dominate, but at the same time, the proportion of large-scale climate factors features gradually increases, indicating that climate change between different seasons may play an important regulatory role in the composition of drought-influencing factors features.



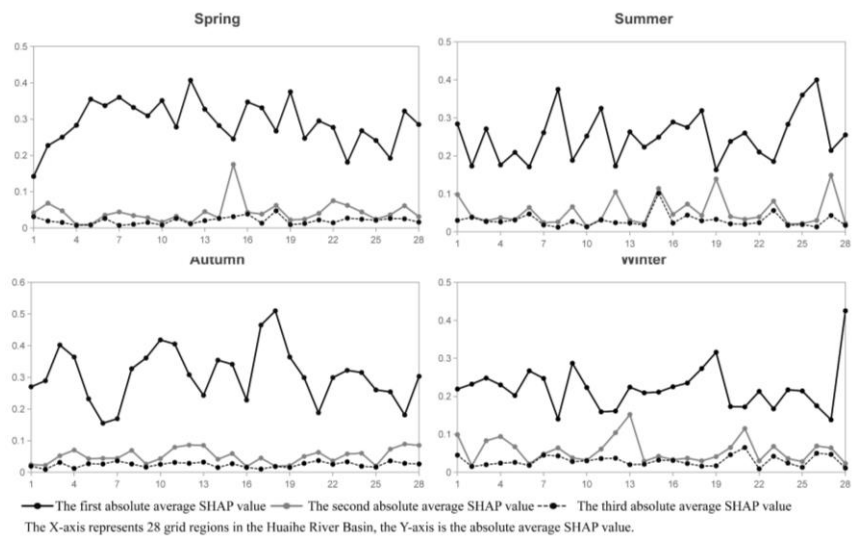


Figure 211: The absolute average SHAP values of the first three drought-influencing factors in each season (The X-axis represents 28 grid regions in the Huaihe River Basin).

5 Discussion

This study demonstrates the efficacy of an XGBoost-SHAP framework for hydrological drought prediction in the Huaihe River Basin. The model achieveds robust accuracy for the ND and D1 categories, yet underperformeds for the more severe categories (D2 and D3), likely due to limited extreme event samples. The prediction of a —one1—month lead time is helpful for drought monitoring. This enables 3

批注 [李敏3]: 横坐标要在图中显示

enabling water managers to adjust reservoir operations and irrigation schedules based on predicted drought conditionsup to date drought classifications. The framework can provides a 30-day buffer for proactive measures, such as mobilizing drought relief resources and implementing crop recommendations.

524

525

526

527

528

529

530

531

532

533534

535

536

537

538

539

540

541

542

543

544

545546

547

548

549

550

551

552

553

SHAP analysis based on the XGBoost model unequivocally identifies the SPI as the most influential predictor of hydrological drought across the Huaihe River Basin. Such as (Tanriverdi and Batmaz, 2025) for U.S. drought prediction, also identified SPI as one of the most critical features across diverse regions and advanced models. Their SHAP analysis consistently ranked SPI among the top predictors, reinforcing its fundamental role as a primary driver of drought conditions, even within sophisticated deep learning frameworks. Beyond SPI, the key secondary drivers exhibit a distinct spatial and seasonal differences. In terms of space, the hydrological drought in the northern part of the basin shows higher sensitivity to large-scale climate oscillations such as AMO, indicating that large-scale climate factors features regulate regional precipitation patterns (Yu et al., 2024). On the contrary, the secondary factorsfeatures affecting the hydrological drought in the southern part of the basin are mainly surface processes, especially soil moisture and evapotranspiration.(Mtupili et al., 2025; Zhu et al., 2025). The difference in the second influencing factors features of hydrological drought in the southern and northern parts of the basin may be due to the fact that the basin belongs to the temperate-subtropical transition position. For the seasonal scale, in spring, soil moisture and evapotranspiration account for a large proportion of the explanatory power of the model. In summer, the relative weight of large-scale climatic factors features increases, which is consistent with the enhancement of water vapor transport (Yu et al., 2024). In autumn and winter, radiative fluxes (net solar and thermal radiation) assume greater importance (Jin et al., 2025). Collectively, these findings underscore SPI as the primary driver while revealing the nuanced spatio-temporal controls exerted by secondary factors features, thereby providing a scientific foundation for developing more targeted drought mitigation and water resource management strategies across the diverse Huaihe River Basin.

When studying the influence of large-scale climate indices on drought, the correlation between climate indices and drought for the same period and a certain lead time is often considered, and the results show that climate indices for the same period and different lead times have a certain influence on drought in the basin, and the degree of influence varies with the changes in the study area. For example, Ren et al. (2017) studied the correlation between SPI and large-scale climate indices with advance periods of 0,

1, 2, and 3 months, and the correlation results show that Nino3.4 has significant correlation in August-October, and PDO has significant correlation in January-May and June-December of the same period. Lv et al. (2022) analyzed the correlation between large-scale climatic factors features and drought in different lag periods. The results show that large-scale climatic factors features in the same period also have an impact on drought. Due to the many influencing factors features considered in this paper, only the effect of climate indices on drought in the basin during the same period was considered when selecting the large-scale climate indices. Subsequent studies can consider selecting the most relevant large-scale climate factors features in different months or seasons as the influencing factors features for basin drought prediction to further improve the accuracy of drought prediction. Before inputting the influencing factors features into the machine learning model for training, methods such as random forest and principal component analysis (PCA) can be used to select the influencing factors features. Future research can extend the existing one-month-ahead framework to multiple prediction periods to evaluate the impact of different lead times on prediction accuracy. To improve the robustness of the model, a variety of ensemble learning schemes can be compared. Furthermore, the introduction of uncertainty quantification and data enhancement helps to alleviate category imbalances and improve prediction reliability. The application of these methods can optimize the influencing factors and provide strong support for more accurate drought trend prediction and management strategies.

6 Conclusions

554555

556

557

558

559

560

561

562

563564

565

566

567

568

569

570

571

572

573574

575

576

577

578

579 580

581

Drought is one of the most significant environmental and climate problems in the world, and drought prediction is a crucial means of drought prevention. In this study, the integration of SHAP and XGBoost provides a novel framework that can not only improve the prediction accuracy, but also show the impact of different drought influencing factors features on drought. The framework can provide two types of support for decision makers: (1) giving priority to high weight factors features in real-time drought warning; (2) Identifying early risk signals in long-term water resources planning. The main conclusions are as follows:

1) The XGBoost model achieved an accuracy of 79.9% for identifying drought elassescategories. The model performs particularly well in predicting ND and D1 drought elassescategories, with a precision rate of 88 % and 74 %, respectively. It also has a recall rate of

$91\ \%$ and $78\ \%$. However, the prediction performance of the model for the D2 and D3 drought
elassescategories is relatively poor, especially for the D3 drought, the recall rate should not exceed
0.5, indicating that the recognition sensitivity of the model for the D3 elasscategory is limited. In
general, the model has high prediction reliability for ND and D1 elassescategories, but limits in the
prediction performance of D2 and D3 classes categories.

- 2) This study determined that SPI is the most critical factor affecting hydrological drought in the Huaihe River Basin. In 28 grid regions, the absolute average SHAP value of SPI is not less than 0.147, which is much higher than other influencing factors features. In addition, large-scale climate factors features, soil moisture content, and evapotranspiration play a significant role in hydrological drought in the basin.
- 3) The SPI remains a major influence in all seasons with absolute average SHAP values of 0.360, 0.261, 0.169, and 0.247 in spring, summer, autumn, and winter respectively. Additional factors features such as soil moisture content, net heat radiation, and solar radiation also play seasonal roles. Soil moisture content and evapotranspiration are significant factors features in spring and autumn, while temperature and large-scale climate factors features are critical in summer and winter.

Reference

- Ardabili, S., Mosavi, A., Dehghani, M., and Várkonyi-Kóczy, A. R.: Deep Learning and Machine Learning in Hydrological Processes Climate Change and Earth Systems a Systematic Review, Cham, 52–62, 2020.
 - Bachmair, S., Svensson, C., Hannaford, J., Barker, L. J., and Stahl, K.: A quantitative analysis to objectively appraise drought indicators and model drought impacts, Hydrol. EARTH Syst. Sci., 20, 2589–2609, https://doi.org/10.5194/hess-20-2589-2016, 2016.
- Barnwal, A., Cho, H., and Hocking, T.: Survival Regression with Accelerated Failure Time Model in XGBoost, J. Comput. Graph. Stat., 31, 1292–1302,
- 607 https://doi.org/10.1080/10618600.2022.2067548, 2022.
- Chen, T. and Guestrin, C.: XGBoost: A Scalable Tree Boosting System, in: Proceedings of the 22nd ACM
 SIGKDD International Conference on Knowledge Discovery and Data Mining, New York, NY,

设置了格式:字体:(默认) Times New Roman, 10 磅 带格式的:缩进:左侧: 0 厘米,悬挂缩进:2 字符,首行缩进:-2 字符,段落间距段后:0 磅,不要在相同样式的段落间增加间距,行距:1.5 倍行距

- 610 USA, event-place: San Francisco, California, USA, 785-794,
- 611 https://doi.org/10.1145/2939672.2939785, 2016.
- 612 Choi, H.-S., Kim, S., Oh, J. E., Yoon, J. E., Park, J. A., Yun, C.-H., and Yoon, S.: XGBoost-Based
- 613 Instantaneous Drowsiness Detection Framework Using Multitaper Spectral Information of
- Electroencephalography, Washington, DC, USA, https://doi.org/10.1145/3233547.3233567, 2018.
- 615 Dai, A.: Characteristics and trends in various forms of the Palmer Drought Severity Index during 1900-
- 616 2008, J. Geophys. Res.-ATMOSPHERES, 116, D12115, https://doi.org/10.1029/2010JD015541,
- 617 2011.
- Dai, A.: Erratum: Drought under global warming: a review, WILEY Interdiscip. Rev.-Clim. CHANGE,
- 619 3, 617–617, https://doi.org/10.1002/wcc.190, 2012.
- 620 Dai, A.: Increasing drought under global warming in observations and models (vol 3, pg 52, 2013), Nat.
- 621 Clim. CHANGE, 3, 171–171, https://doi.org/10.1038/NCLIMATE1811, 2013.
- 622 Dikshit, A. and Pradhan, B.: Interpretable and explainable AI (XAI) model for spatial drought prediction,
- 623 Sci. TOTAL Environ., 801, 149797, https://doi.org/10.1016/j.scitotenv.2021.149797, 2021.
- 624 Fu, Q., Zhou, Z., Li, T., Liu, D., Hou, R., Cui, S., and Yan, P.: Spatiotemporal characteristics of droughts
- and floods in northeastern China and their impacts on agriculture, Stoch. Environ. Res. RISK
- 626 Assess., 32, 2913–2931, https://doi.org/10.1007/s00477-018-1543-z, 2018.
- 627 Gan, R., Li, D., Chen, C., Yang, F., Zhang, X., and Guo, X.: Spatiotemporal characteristics of extreme
- hydrometeorological events and its potential influencing factors in the Huaihe River Basin, China,
- 629 Stoch. Environ. Res. RISK Assess., 37, 2693–2712, https://doi.org/10.1007/s00477-023-02413-4,
- 630 2023.
- 631 Gao, L. and Ding, Y.: Disease prediction via Bayesian hyperparameter optimization and ensemble
- learning, BMC Res. NOTES, 13, 205, https://doi.org/10.1186/s13104-020-05050-0, 2020.
- 633 Gunning, D., Stefik, M., Choi, J., Miller, T., Stumpf, S., and Yang, G.-Z.: XAI-Explainable artificial
- intelligence, Sci. Robot., 4, eaay7120, https://doi.org/10.1126/scirobotics.aay7120, 2019.
- Han, Y., Wu, J., Zhai, B., Pan, Y., Huang, G., Wu, L., and Zeng, W.: Coupling a Bat Algorithm with
- XGBoost to Estimate Reference Evapotranspiration in the Arid and Semiarid Regions of China,
- 637 Adv. Meteorol., 2019, 9575782, https://doi.org/10.1155/2019/9575782, 2019.
- 638 Heidke, P.: Berechnung Des Erfolges Und Der Güte Der Windstärkevorhersagen Im
- 639 Sturmwarnungsdienst, Geogr. Ann., 8, 301–349, https://doi.org/10.1080/20014422.1926.11881138,

- 640 1926.
- 641 Islam, M. R., Ahmed, M. U., Barua, S., and Begum, S.: A Systematic Review of Explainable Artificial
- Intelligence in Terms of Different Application Domains and Tasks, Appl. Sci.-BASEL, 12, 1353,
- 643 <u>https://doi.org/10.3390/app12031353</u>, 2022.
- 644 Jin, H., Zhang, K., Zhang, P., Liu, G., Liu, M., Chen, X., and Willems, P.: Spatiotemporal evolution of
- drought status and its driving factors attribution in China., Sci. Total Environ., 958, 178131–178131,
- https://doi.org/10.1016/j.scitotenv.2024.178131, 2025.
- 547 Jungho, S. and Kim, Y.: Assessing the likelihood of drought impact occurrence with extreme gradient
- boosting: a case study on the public water supply in South Korea, J. HYDROINFORMATICS, 25,
- 649 191–207, https://doi.org/10.2166/hydro.2023.064, 2023.
- 650 Kikon, A. and Deka, P. C.: Artificial intelligence application in drought assessment, monitoring and
- forecasting: a review, Stoch. Environ. Res. RISK Assess., 36, 1197-1214,
- 652 <u>https://doi.org/10.1007/s00477-021-02129-3</u>, 2022.
- 653 Li, J., Wang, Z., Wu, X., Xu, C.-Y., Guo, S., Chen, X., and Zhang, Z.: Robust Meteorological Drought
- Prediction Using Antecedent SST Fluctuations and Machine Learning, WATER Resour. Res., 57,
- e2020WR029413, https://doi.org/10.1029/2020WR029413, 2021.
- 656 Li, M., Feng, Z., Zhang, M., and Yao, Y.: Influence of large-scale climate indices and regional
- meteorological elements on drought characteristics in the Luanhe River Basin, ATMOSPHERIC
- Res., 300, 107219, https://doi.org/10.1016/j.atmosres.2024.107219, 2024.
- 659 Lu, R., Dong, B., and Ding, H.: Impact of the Atlantic Multidecadal Oscillation on the Asian summer
- 660 monsoon, Geophys. Res. Lett., 33, https://doi.org/10.1029/2006GL027655, 2006.
- 661 Lundberg, S. M. and Lee, S.-I.: A Unified Approach to Interpreting Model Predictions, in: Advances in
- Neural Information Processing Systems, 2017.
- 663 Lv, A., Fan, L., and Zhang, W.: Impact of ENSO Events on Droughts in China, Atmosphere, 13,
- https://doi.org/10.3390/atmos13111764, 2022.
- 665 Mardian, J., Champagne, C., Bonsal, B., and Berg, A.: A Machine Learning Framework for Predicting
- and Understanding the Canadian Drought Monitor, WATER Resour. Res., 59, e2022WR033847,
- https://doi.org/10.1029/2022WR033847, 2023.
- McKee, T. B., Doesken, N. J., and Kleist, J.: THE RELATIONSHIP OF DROUGHT FREQUENCY
- AND DURATION TO TIME SCALES, 1993.

- 670 Mishra, A. K. and Singh, V. P.: A review of drought concepts, J. Hydrol., 391, 204-216,
- 671 https://doi.org/10.1016/j.jhydrol.2010.07.012, 2010.
- 672 Molnar, C.: Interpretable Machine Learning: A Guide for Making Black Box Models Explainable, 2nd
- 673 ed., 2022.
- 674 Mtupili, M., Wang, R., Gu, L., and Yin, J.: Delayed Response of Soil Moisture and Hydrological
- Droughts to Meteorological Drought Over East Asia, Int. J. Climatol.,
- 676 <u>https://doi.org/10.1002/joc.8883</u>, 2025.
- Orimoloye, I. R., Ololade, O. O., and Belle, J. A.: Satellite-based application in drought disaster
- 678 assessment using terra MOD13Q1 data across free state province, South Africa, J. Environ. Manage.,
- 679 285, 112112, https://doi.org/10.1016/j.jenvman.2021.112112, 2021.
- Orimoloye, I. R., Olusola, A. O., Belle, J. A., Pande, C. B., and Ololade, O. O.: Drought disaster
- 681 monitoring and land use dynamics: identification of drought drivers using regression-based
- algorithms, Nat. HAZARDS, 112, 1085–1106, https://doi.org/10.1007/s11069-022-05219-9, 2022.
- 683 Park, H., Kim, K., and Lee, D. K.: Prediction of Severe Drought Area Based on Random Forest: Using
- Satellite Image and Topography Data, WATER, 11, 705, https://doi.org/10.3390/w11040705, 2019.
- Phan-Van, T., Nguyen-Ngoc-Bich, P., Ngo-Duc, T., Vu-Minh, T., Le, P. V. V., Trinh-Tuan, L., Nguyen-
- Thi, T., Pham-Thanh, H., and Tran-Quang, D.: Drought over Southeast Asia and Its Association with
- 687 Large-Scale Drivers, J. Clim., 35, 4959–4978, https://doi.org/10.1175/JCLI-D-21-0770.1, 2022.
- 688 Prodhan, F. A., Zhang, J., Hasan, S. S., Sharma, T. P. P., and Mohana, H. P.: A review of machine learning
- 689 methods for drought hazard monitoring and forecasting: Current research trends, challenges, and
- 690 future research directions, Environ. Model. Softw., 149, 105327,
- 691 <u>https://doi.org/10.1016/j.envsoft.2022.105327</u>, 2022.
- Raposo, V. de M. B., Costa, V. A. F., and Rodrigues, A. F.: A review of recent developments on drought
- characterization, propagation, and influential factors, Sci. Total Environ., 898, 165550,
- 694 <u>https://doi.org/10.1016/j.scitotenv.2023.165550</u>, 2023.
- 695 Ren, W., Wang, Y., Li, J., Feng, P., and Smith, R. J.: Drought forecasting in Luanhe River basin involving
- climatic indices, Theor. Appl. Climatol., 130, 1133–1148, https://doi.org/10.1007/s00704-016-
- 697 1952-1, 2017.
- 698 Ribeiro, M. T., Singh, S., and Guestrin, C.: Model-Agnostic Interpretability of Machine Learning, 2016a.
- 699 Ribeiro, M. T., Singh, S., and Guestrin, C.: "Why Should I Trust You?": Explaining the Predictions of

- Any Classifier, in: Proceedings of the 22nd ACM SIGKDD International Conference on Knowledge
- 701 Discovery and Data Mining, New York, NY, USA, event-place: San Francisco, California, USA,
- 702 1135–1144, https://doi.org/10.1145/2939672.2939778, 2016b.
- 703 Shapley, L. S.: 17. A Value for n-Person Games, in: Contributions to the Theory of Games (AM-28),
- Volume II, edited by: Kuhn, H. W. and Tucker, A. W., Princeton University Press, Princeton, 307-
- 705 318, https://doi.org/doi:10.1515/9781400881970-018, 1953.
- 706 Shi, H., Chen, J., Wang, K., and Niu, J.: A new method and a new index for identifying socioeconomic
- 707 drought events under climate change: A case study of the East River basin in China, Sci. TOTAL
- 708 Environ., 616, 363–375, https://doi.org/10.1016/j.scitotenv.2017.10.321, 2018.
- Nukla, S. and Wood, A. W.: Use of a standardized runoff index for characterizing hydrologic drought,
- 710 Geophys. Res. Lett., 35, L02405, https://doi.org/10.1029/2007GL032487, 2008.
- 711 Sun, A. Y. and Scanlon, B. R.: How can Big Data and machine learning benefit environment and water
- 712 management: a survey of methods, applications, and future directions, Environ. Res. Lett., 14,
- 713 073001, https://doi.org/10.1088/1748-9326/ab1b7d, 2019.
- 714 Sun, P., Sun, Y., Zhang, Q., and Yao, R.: Hydrological Processes in the Huaihe River Basin, China:
- 715 Seasonal Variations, Causes and Implications, Chin. Geogr. Sci., 28, 636-653,
- 716 <u>https://doi.org/10.1007/s11769-018-0969-z</u>, 2018.
- 717 Tanriverdi, I. and Batmaz, I.: AI-driven US drought prediction using machine learning and deep learning,
- 718 Clim. Dyn., 63, 249, https://doi.org/10.1007/s00382-025-07720-w, 2025.
- Wang, J., Wang, W., Cheng, H., Wang, H., and Zhu, Y.: Propagation from Meteorological to Hydrological
- 720 Drought and Its Influencing Factors in the Huaihe River Basin, WATER, 13, 1985,
- 721 https://doi.org/10.3390/w13141985, 2021.
- 722 Wu, Y. and Xu, Y.: Assessing the Climate Tendency over the Yangtze River Delta, China: Properties,
- Dry/Wet Event Frequencies, and Causes, Water, 12, https://doi.org/10.3390/w12102734, 2020.
- 724 Wu, Z., Yin, H., He, H., and Li, Y.: Dynamic-LSTM hybrid models to improve seasonal drought
- 725 predictions over China, J. Hydrol., 615, 128706, https://doi.org/10.1016/j.jhydrol.2022.128706,
- 726 2022.
- 727 Xiao, L., Chen, X., Zhang, R., and Zhang, Z.: Spatiotemporal Evolution of Droughts and Their
- 728 Teleconnections with Large-Scale Climate Indices over Guizhou Province in Southwest China,
- 729 Water, 11, https://doi.org/10.3390/w11102104, 2019.

- 730 Xu, D., Zhang, Q., Ding, Y., and Zhang, D.: Application of a hybrid ARIMA-LSTM model based on the
- 731 SPEI for drought forecasting, Environ. Sci. Pollut. Res., 29, 4128-4144,
- 732 <u>https://doi.org/10.1007/s11356-021-15325-z</u>, 2022.
- 733 Xue, C., Ghirardelli, A., Chen, J., and Tarolli, P.: Investigating agricultural drought in Northern Italy
- 734 through explainable Machine Learning: Insights from the 2022 drought, Comput. Electron. Agric.,
- 735 227, 109572, https://doi.org/10.1016/j.compag.2024.109572, 2024.
- 736 Yalcin, S., Esit, M., and Coban, O.: A new deep learning method for meteorological drought estimation
- 737 based-on standard precipitation evapotranspiration index, Eng. Appl. Artif. Intell., 124, 106550,
- 738 <u>https://doi.org/10.1016/j.engappai.2023.106550</u>, 2023.
- 739 Yu, J., Li, Q., Ding, Y., Wen, Z., Gong, Z., Sun, X., Shen, X., and Dong, L.: AMO modulation of
- 740 interdecadal background of persistent heavy rainfall in summer over the Huaihe River Basin, Clim.
- 741 Dyn., 62, 3621–3640, https://doi.org/10.1007/s00382-023-07088-9, 2024.
- 742 Yu, Q., Jiang, L., Wang, Y., and Liu, J.: Enhancing streamflow simulation using hybridized machine
- 743 learning models in a semi-arid basin of the Chinese loess Plateau, J. Hydrol., 617, 129115,
- 744 <u>https://doi.org/10.1016/j.jhydrol.2023.129115</u>, 2023.
- 745 Zeng, X.-M., Nie, M., Wang, N., Ullah, I., Bai, G., Wang, M., Zhang, Z., and Zhu, J.: Attributing
- 746 spatiotemporal evolution and driving factors of meteorological drought across Yangtze River Basin,
- 747 China, ATMOSPHERIC Res., 323, 108155, https://doi.org/10.1016/j.atmosres.2025.108155, 2025.
- 748 Zhang, B., Abu Salem, F. K., Hayes, M. J., Smith, K. H., Tadesse, T., and Wardlow, B. D.: Explainable
- 749 machine learning for the prediction and assessment of complex drought impacts, Sci. TOTAL
- 750 Environ., 898, 165509, https://doi.org/10.1016/j.scitotenv.2023.165509, 2023.
- 751 Zhang, R., Chen, Z.-Y., Xu, L.-J., and Ou, C.-Q.: Meteorological drought forecasting based on a
- 752 statistical model with machine learning techniques in Shaanxi province, China, Sci. TOTAL
- 753 Environ., 665, 338–346, https://doi.org/10.1016/j.scitotenv.2019.01.431, 2019.
- 754 Zhou, Z., Shi, H., Fu, Q., Li, T., Gan, T. Y., and Liu, S.: Assessing spatiotemporal characteristics of
- 755 drought and its effects on climate-induced yield of maize in Northeast China, J. Hydrol., 588,
- 756 125097, https://doi.org/10.1016/j.jhydrol.2020.125097, 2020.
- 757 Zhou, Z., Shi, H., Fu, Q., Ding, Y., Li, T., and Liu, S.: Investigating the Propagation From Meteorological
- 758 to Hydrological Drought by Introducing the Nonlinear Dependence With Directed Information
- 759 Transfer Index, WATER Resour. Res., 57, e2021WR030028,

761	Zhu, S., Huang, W., Wei, Y., Guo, J., and Qin, H.: Impact of driving factors on drought propagation:
762	perspectives on rainfall deficit and excessive evaporation, Clim. Dyn., 63, 204,
763	https://doi.org/10.1007/s00382-025-07618-7, 2025.
764	Zou, L., Xia, J., and She, D.: Analysis of Impacts of Climate Change and Human Activities on
765	Hydrological Drought: a Case Study in the Wei River Basin, China, WATER Resour. Manag., 32,
766	1421–1438, https://doi.org/10.1007/s11269-017-1877-1, 2018.
767	Statements & Declarations
768	Software and data availability
769	The code and data set for prediction using python language (version 3.9.13) can be found in Mendeley
770	Data: doi: 10.17632 / $jnr2z36g77.1$. The warehouse was created by Yuhang Yao (e-mail: 151746151 @
771	qq.com). The author 's experimental environment is as follows:
772	CPU: AMD Ryzen 9 7845HX 3.00 GHz;
773	GPU: NVIDIA GeForce RTX4060 8 GB;
774	RAM:16G.
775	Funding
,,,	
776	This work was supported by the Open Fund of State Key Laboratory of Water Disaster Prevention (No.
	This work was supported by the Open Fund of State Key Laboratory of Water Disaster Prevention (No. 2024490711), the State Key Laboratory of Hydraulic Engineering Intelligent Construction and Operati
776	
776 777	2024490711), the State Key Laboratory of Hydraulic Engineering Intelligent Construction and Operati
776 777 778	2024490711), the State Key Laboratory of Hydraulic Engineering Intelligent Construction and Operation (No. HESS-2206), and Yangzhou University Graduate Student Research and Practice Innovation
776 777 778 779	2024490711), the State Key Laboratory of Hydraulic Engineering Intelligent Construction and Operation (No. HESS-2206), and Yangzhou University Graduate Student Research and Practice Innovation Program Funding projects (No. SJCX24_2250).
776 777 778 779 780	2024490711), the State Key Laboratory of Hydraulic Engineering Intelligent Construction and Operation (No. HESS-2206), and Yangzhou University Graduate Student Research and Practice Innovation Program Funding projects (No. SJCX24_2250). This work was supported by the State Key Laboratory of Hydraulic Engineering Intelligent Construction
776 777 778 779 780 781	2024490711), the State Key Laboratory of Hydraulic Engineering Intelligent Construction and Operation (No. HESS-2206), and Yangzhou University Graduate Student Research and Practice Innovation Program Funding projects (No. SJCX24_2250). This work was supported by the State Key Laboratory of Hydraulic Engineering Intelligent Construction and Operation (No. HESS-2206), the Open Fund of Key Laboratory of Flood & Drought Disaster
776 777 778 779 780 781 782	2024490711), the State Key Laboratory of Hydraulic Engineering Intelligent Construction and Operation (No. HESS-2206), and Yangzhou University Graduate Student Research and Practice Innovation Program Funding projects (No. SJCX24_2250). This work was supported by the State Key Laboratory of Hydraulic Engineering Intelligent Construction and Operation (No. HESS 2206), the Open Fund of Key Laboratory of Flood & Drought Disaster Defense, the Ministry of Water Resources (KYFB202307260034), and Yangzhou University Graduate
776 777 778 779 780 781 782 783	2024490711), the State Key Laboratory of Hydraulic Engineering Intelligent Construction and Operation (No. HESS-2206), and Yangzhou University Graduate Student Research and Practice Innovation Program Funding projects (No. SJCX24_2250). This work was supported by the State Key Laboratory of Hydraulic Engineering Intelligent Construction and Operation (No. HESS-2206), the Open Fund of Key Laboratory of Flood & Drought Disaster Defense, the Ministry of Water Resources (KYFB202307260034), and Yangzhou University Graduate Student Research and Practice Innovation Program Funding projects (SJCX24_2250).
776 777 778 779 780 781 782 783	2024490711), the State Key Laboratory of Hydraulic Engineering Intelligent Construction and Operation (No. HESS-2206), and Yangzhou University Graduate Student Research and Practice Innovation Program Funding projects (No. SJCX24_2250). This work was supported by the State Key Laboratory of Hydraulic Engineering Intelligent Construction and Operation (No. HESS-2206), the Open Fund of Key Laboratory of Flood & Drought Disaster Defense, the Ministry of Water Resources (KYFB202307260034), and Yangzhou University Graduate Student Research and Practice Innovation Program Funding projects (SJCX24_2250). Competing Interests
776 777 778 779 780 781 782 783 784 785	2024490711), the State Key Laboratory of Hydraulic Engineering Intelligent Construction and Operation (No. HESS-2206), and Yangzhou University Graduate Student Research and Practice Innovation Program Funding projects (No. SJCX24_2250). This work was supported by the State Key Laboratory of Hydraulic Engineering Intelligent Construction and Operation (No. HESS-2206), the Open Fund of Key Laboratory of Flood & Drought Disaster Defense, the Ministry of Water Resources (KYFB202307260034), and Yangzhou University Graduate Student Research and Practice Innovation Program Funding projects (SJCX24_2250). Competing Interests The authors declare no conflict of interest.

760

789

Corresponding author

https://doi.org/10.1029/2021WR030028, 2021.

带格式的: 不要在相同样式的段落间增加间距,行距: 单倍行距 790 Correspondence to Min Li, Mail: limintju@126.com 791 **Author Contributions** All authors contributed this paper: Conceptualization, M L; Data curation, M L, YH Y, ZL F, Ming Ou; 792 793 Visualization, YH Y, M L; Validation, M L, YH Y; Methodology, M L, YH Y, ZL F; Formal Analysis, M 794 L, YH Y; Funding acquisition, M L; Writing – original draft, YH Y; Writing – review & editing, M L. 795 Data availability 796 are grateful to the National Oceanic and Atmospheric Administration 797 (http://www.esrl.noaa.gov/psd/data/climateindices) for providing large-scale climate index data, and 798 grateful to the GLDAS for providing monthly average precipitation, temperature, wind speed, soil water 799 content, evapotranspiration data sets and runoff data sets, and to the European Centre for Medium-Range Weather Forecasts (https://cds.climate.copernicus.eu/) for providing monthly average 2-m dewpoint 800 temperature, surface net solar radiation, surface net thermal radiation, surface pressure, and leaf area 801 802 index data sets. The data and materials of this study are available.